A Steady-State Electrochemical Model of Vascular Smooth Muscle Cells

Masood A. Machingal and S. V. Ramanan
AU-KBC Research Centre, MIT Campus of Anna University, Chromepet, Chennai, India 600044

ABSTRACT A model of the steady-state electrochemical response of vascular smooth muscle cells to external stimuli is presented, which accounts for K, Na, and Ca fluxes. The results of the model are broadly in accordance with experimental data 1), at various transmural pressures; 2), with channel and pump blockade; and 3), under manipulation of external ionic concentrations. The model exhibits dual stable states which sometimes coexist, and abrupt transitions between these states may account for nongraded responses in arteries as external potassium or pressure is varied. The simulations suggest that changes in the intracellular sodium concentration ($[Na]_i$) often accompany smooth muscle responses. For example, $[Na]_i$ values vary threefold over the range of pressures from 10 to 100 mmHg.

INTRODUCTION

The vascular myogenic response is the acute reaction of a blood vessel to a change in transmural pressure. In many tissues, blood flow rate is held at a constant level even as the perfusion pressure changes (1). This autoregulatory response is achieved by two different mechanisms (2), namely: the metabolic mechanism, in which metabolites, such as adenosine and pO_2, act on the blood vessel; and the myogenic mechanism, in which the change in the transmural pressure itself acts on the vessel to maintain a constant blood flow. The myogenic response is independent of neural, metabolic, and hormonal influences and seems to be an inherent characteristic of smooth muscle, being especially pronounced in arterioles (3).

Over the last several decades, numerous investigators have demonstrated the importance of the myogenic response in the local regulation of blood flow and capillary pressure, and in the generation of basal vascular tone (4). The myogenic mechanism has been shown to play a significant role in autoregulation in arteries isolated from various tissues, including cerebral (5) and coronary arteries (6).

The mechanism underlying the myogenic response is thought to be as follows (7). It has been established that increased intravascular pressure causes a graded membrane potential depolarization of smooth muscle cells that line the arterial wall in various tissues (8,9). These tissues include rat middle cerebral arteries (9) and rabbit cerebral arteries (7,10). This depolarization, which probably results from the opening of stretch-activated TRC channels (11), causes voltage-dependent calcium channels to open. The resultant increase in cytosolic calcium, through a series of signaling processes (12), finally activates myosin light chain kinases resulting in the contraction of the cell and constriction of arterial diameter. The increased calcium itself also activates the release of calcium from the sarcoplasmic reticulum as calcium sparks. These sparks activate calcium-activated large potassium (BK) channels, which in turn hyperpolarize the cell. This mechanism acts as a feedback loop to regulate the steady-state membrane potential (7).

The experimental information above has formed the basis for many models of myogenic response. Most of the models reported so far take into account only the mechanical aspects of myogenic response such as phosphorylation, cross-bridge formation, force development, length-tension relationship, vessel resistance, and vessel diameter. For example, the force equilibrium model proposed in Borgstrom et al. (13,14) describes the responses of myogenic vascular resistance to changes in transmural pressure. The kinetic model of cross-bridge phosphorylation and the regulation of latch state in smooth muscle are described in Hai and Murphy (15). Lee et al. (16) described a biomechanical model that was based on the assumption that the arteriolar wall exhibits viscoelastic properties. A minimal model of arterial vasomotion, including the nonlinear interaction of intracellular and membrane calcium oscillators, is developed in Parthimos et al. (17). However, none of the above models encapsulate the cellular electrochemical properties that form the basis of the myogenic response.

The only electrochemical model of smooth muscle is a kinetic model that incorporates membrane channels and transporters (18) as well as mechanical components of cell response during the development of tension. The results of the model (18) were compared (19) against the experimental results reported in Knot et al. (7) and Knot and Nelson (10). In these experiments, the myogenic response was studied in intact cannulated cerebral arteries. The calcium levels, the membrane potential, and the arterial diameter of pressurized small cerebral arteries were simultaneously measured. These data led to the observation that cytosolic calcium depended only on the membrane potential. The results in Yang et al. (19) mimic the experimental data for steady-state membrane

Submitted December 1, 2005, and accepted for publication May 19, 2006.

Address reprint requests to S. V. Ramanan, Tel.: 91-44-223-4885; Fax: 91-44-2-223-1034; E-mail: ramanan@au-kbc.org.

Masood A. Machingal's present address is Virginia Tech-Wake Forest University School of Biomedical Engineering and Sciences, Medical Center Boulevard, Winston-Salem, NC 27157.

0006-3495/06/09/1648/15 $2.00

doi: 10.1529/biophysj.105.078923

potential and arterial diameter, but not for intracellular calcium.

The steady-state myogenic response is reached in a path-independent manner, as reflected, e.g., in the fact that it is the same when either pressure steps or pressure ramps are used to elicit tone (20). We have therefore attempted in this work to model the smooth muscle only in the steady state. The model is a purely electrochemical representation of the changes in the vascular smooth muscle cell in response to applied pressure. We do not model the mechanical responses of the cell in response to the changes in calcium and potential. However, the model can be used to calculate changes in the membrane potential as well as the calcium concentrations in response to applied pressures, as well as in response to channel and transporter antagonists.

The model (Fig. 1) incorporates L-type calcium channels, calcium pumps, inward rectifiers, sodium-calcium exchangers, sodium-potassium pumps, and stretch currents. We have specifically considered processes with long time constants that would be important in setting steady-state myogenic tone. The model has an inbuilt feedback loop for the potential (7) through the dependence of calcium-activated maxi-K potassium channels on calcium sparks. The intrinsic channel and pump parameter values in the model are very close to those reported in the literature. The model is able to mimic the experimental data on the steady-state characteristics of vascular smooth muscle cells under a variety of experimental conditions, including pressure, channel and pump block, and variation in extracellular ionic concentrations.

MATERIALS AND METHODS

We consider only the major cations in the vascular smooth muscle cell (VSMC), namely calcium (Ca), potassium (K), and sodium (Na). The ionic concentrations at rest are determined by the coordinated function of the various pumps, channels and transporters in the cell. These concentrations, in turn, set the basal myogenic tone. When an external stimulus (e.g., external pressure, stretch) is applied, the cell shifts to a new steady state. At steady-state condition, net transmembrane flux of each ion is zero.

Calcium fluxes across the sarcoplasmic reticulum (SR)

Calcium pumps and release mechanisms such as ryanodine receptors and IP_3 receptors are present in the sarcoplasmic reticulum (SR), and affect calcium dynamics. The activity of the pumps and channels in the SR membrane may vary with the intracellular calcium concentration ($[Ca]_i$). However, the SR is a finite source, and in the steady state, uptake and release across the SR membrane must be equal. This implies that the calcium concentration inside the SR is not a free variable in the steady state, but is determined by $[Ca]_i$.

It is known (21) that calcium sparks, which originate in the SR, activate calcium-activated BK channels and thereby influence the membrane potential. However, it has been shown experimentally that the frequency of the sparks is a function only of the membrane potential under the physiological range of transmural pressures (22,23). We therefore do not explicitly include the SR in the calculation of $[Ca]_i$.

Ionic currents

The complete set of equations that describe the ionic currents through the various channels, transporters and pumps in the model are given in the Appendix. The parameters in these equations are of two kinds:

- The intrinsic parameters that describe the dependence of the current on membrane potential, pressure, or ionic concentrations. Almost all of these parameters are taken directly from the literature (Table 1). The exceptions are two parameters that describe the response to pressure of the stretch channel.
- The extrinsic parameters, such as peak conductance or maximal pump current, which reflect the number of channels, pumps, or transporters (Table 2). The seed values for these extrinsic parameters were taken or derived from the literature, as detailed below. The steady-state condition that transmembrane flux of all the three cations be zero over a range of pressures implies that the values for these parameters cannot be set independently. Hence their values were set by a fitting procedure detailed in Estimation Parameters and Justification, below.

In the following descriptions of the individual ionic currents, the label (*a*) is used to describe intrinsic parameters and the label (*b*) is used for text that justifies the seed values for the extrinsic parameters.

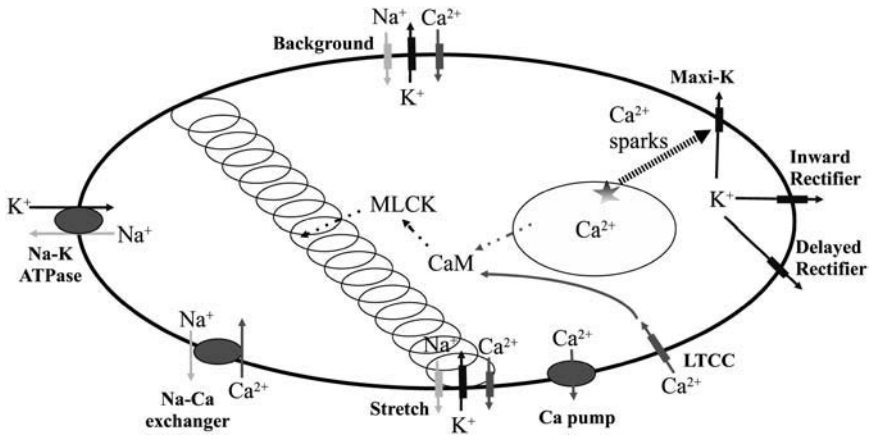

FIGURE 1 Schematic of the major ionic currents in the model. An increase in membrane or cytoskeletal tension opens stretch-activated channels. This stretch-activated current (I_s), which is primarily due to Na^+ influx, depolarizes the membrane. Depolarization opens L-type Ca^{2+} channels (LTCC), and the resultant Ca^{2+} influx (I_l) activates downstream effects. In the steady state, this Ca^{2+} influx is balanced by efflux across the calcium pump (I_{CaP}). Increased intracellular Ca^{2+} increases calcium spark frequency which, in turn, activates K^+ influx through Maxi-K channels (I_{bk}). This current, as well as the K^+ current though the delayed rectifier channel (I_{dr}), act as feedback loops to limit depolarization in the steady state. The outward K^+ current through inward rectifiers (I_{ir}) is bell-shaped as a function of membrane potential, and causes bistable states in the model. Electrogenic Na-K pumps (I_{NaK}) and Na-Ca exchangers (I_{NCX}) act as coupling elements between the three cationic fluxes. Pathways shown as dashed lines are downstream effects due to increased intracellular calcium, and are not considered in the model. These downstream effects result in cell contraction induced by myosin light-chain kinase activation via a calcium-calmodulin complex.

TABLE 1 Ionic current formulations from previous studies

Current	Components	New parameter values	Reference
I_l	All except b_l	No change	(24)
	b_l*	No change	(26,27)
I_s	All	No change	(18,31)
I_{cp}	All	No change	(34)
I_{NCX}	All except r	No change	(38,39)
	$r^\dagger$	No change	(40)
I_{dr}	All	No change	(42,43)
I_{ir}	All except $\theta^\ddagger$	slope = 8.1 mV	(44)
	$\theta^\S$		(26,27)
I_{bk}	All except P'_{bk}	No change	(22,45)
	P'_{bk}¶	No change	(23)
I_{NaK}	All	No change	(47,60)
I_b	All	No change	(18)

Table 1 lists all the components in the various ionic currents in the model, along with the primary references. The parameter values that describe the dependence of these currents on membrane potential, calcium, or other ionic concentrations are taken directly from these references.

*b_l is block of LTCC by $[Ca]_i$.

†r is block of reverse-mode activity of NCX by $[Na]_o$.

‡See text.

§θ is outward currents through the IR channel; see Fig. 2.

¶P'_{bk} is dependence of spark frequency on $[Ca]_i$.

Voltage-operated L-type calcium channel, I_l

(*a*) Equations and intrinsic parameters describing the voltage-dependence of L-type Ca^{2+} channels (LTCCs) are taken from Rubart et al. (24); these are based on whole-cell current data in smooth muscle from rat cerebral resistance arteries. The equations in Rubart et al. (24) do not take into account the observation that high $[Ca]_i$ blocks LTCCs in VSMCs with an IC_{50} of 380 nM and a Hill coefficient of 3 (25); however, with these parameter values, the model results for $[Ca]_i$ were far below the experimental results. We used the values in the L-R model for cardiac myocytes (26,27), namely an IC_{50} of 600 nM and a Hill coefficient of 2.

(*b*) The conductance g_l was seeded to a value of 17.5 nS.

Stretch-operated channels, $I_{s,c}$

(*a*) The experimental data (11,28,29) indicate that pressure-induced depolarization results from the opening of stretch-activated nonspecific cation channels. Single-channel and macroscopic currents have been measured during mechanical stimulation of vascular smooth muscle from coronary arteries (30). The stretch current is primarily carried by sodium ions, but with contributions from potassium and calcium ions (31). We represent the current across the open channel based on the GHK equation, as previously proposed (18). The pressure- (or stretch-) dependence of the current is modeled as a Boltzmann (18). There are no experimental data on the parameters of the Boltzmann that describe the pressure-current relation. These two intrinsic parameters alone were also estimated by fitting. As VSMCs exhibit a basal tone, we seeded the half-maximal stretch to correspond to the stress induced by a basal isobaric pressure of 60 mmHg ($\sigma_{1/2}$ = 240 mmHg). The relationship between stress and transmural pressure is described below. The parameter k_σ defines the operational stress-sensing range of the stretch channel; we seeded this range to a stress of 140 mmHg (or 35 mmHg of pressure).

(*b*) A half-maximal inward current of 100 pA is activated by stretching single VSMCs (30). Using this information with the GHK equation gave a seed conductance g_s of 0.14 pA/mM.

Calcium extrusion pump, I_{cp} or I_{CaP}

(*a*) The Ca-ATPase has been studied in smooth muscle cells (32). Ca-ATPase pumps are stimulated by calmodulin, which itself binds four calcium ions (33). The binding is known to be cooperative, with a Hill coefficient of 4 and a half-maximal concentration of 300 nM (34). We have assumed that the pump activity is linearly related to the concentration of the calcium-calmodulin complex.

(*b*) The basal transmembrane calcium flux in isolated smooth muscle cells is 10^{-18} moles/s/cell (35). $[Ca]_i$ at low transmural pressures is 100 nM (10). This yields a seed value for the maximal flux $I_{0,cp}$ of 8.2 pA.

Sodium calcium exchanger, I_{NCX}

(*a*) While there is extensive data on the Na-Ca exchanger (NCX) in cardiac cells, there is limited literature that directly characterizes this exchanger in vascular smooth muscle (36,37). We have therefore followed the formalism used in modeling the NCX in cardiac myocytes (38,39). The model also takes into account the observation that high extracellular sodium ($[Na]_o$) blocks the reverse-mode activity of the NCX with a Hill coefficient of 2 and a K_d of 60 mM (40).

(*b*) The maximum flux ($\bar{I}_{NCX}$) has a value of 2.5×10^{-4} pA/(mM)^4 in cardiac myocytes (39). $\bar{I}_{NCX}$was seeded to 2×10^{-5} to reflect the observation that the Na-Ca exchanger plays only a supportive role when $[Na]_i$ is kept at physiological levels (37,41).

Delayed rectifier channel, I_{dr}

(*a*) Equations and parameters for this channel have been described (42,43).

(*b*) Using the estimate of 1000 channels with a single-channel conductance of 7 pS (42), the peak conductance g_{dr} was seeded to 7 nS.

TABLE 2 Seed and final values of the variable parameters in the model

Parameter	Definition	Seed	Final	Units
g_l	Peak I_l conductance	17.5	3.03	nS
g_s	Peak I_s conductance	0.14	0.28	pA/mM
$\sigma_{1/2}$	Half-maximal membrane tension for I_s	240	548	mmHg
k_σ	Inverse slope for I_s	140	108.7	mmHg
$I_{o,cp}$	Maximum Ca pump current	8.2	14.32	pA
$\bar{I}_{NCX}$	Maximum NCX current	2×10^{-5}	8.7×10^{-5}	pA/(mM)^4
g_{dr}	Peak I_{dr} conductance	7	2.4	nS
g_{ir}	Peak I_{ir} conductance	0.145	0.272	nS/(mM)$^{0.5}$
g_{bk}	Peak I_{bk} conductance	0.6	2.54	nS
$\bar{I}_{NaK}$	Maximum Na-K pump current	20	20	pA

Table 2 shows the seed and the final values for all the variable parameters in the model. Seed values were taken from the literature as described in the text. Two of these parameters, namely $\sigma_{1/2}$ and k_σ, characterize the midpoint and steepness of the response of the stretch channel. All the other parameters relate to channel conductances or maximal flux across pumps or transporters.

Inward rectifier channel, I_{ir}

(*a*) The equations for inward currents across the inward rectifier (IR) channel are based on an existing formulation (44), except that the inverse slope of the Boltzmann was increased from 6.9 to 8.1 mV. Outward currents through the IR channel in VSMCs are less well characterized, as they are quite small (44). Fig. 2 shows the open probability P_{ir} in the model (*dashed lines*) as a function of the membrane potential (V_m, positive to E_K); also plotted are the pure Boltzmann probability p_{ir} below (*solid lines*) as well as the probability in the L-R model (*dotted lines*) for cardiac myocytes (26,27). The open probability P_{ir} differs from a Boltzmann through the incorporation of an extra term θ. The effect of the term θ is to introduce a small dip in the outward current at ~15 mV positive of E_k; this changes the stability of the model slightly at very low pressures and is discussed in Results, below.

(*b*) The initial value of the conductance G_{ir} was set to $0.145\,\mathrm{nS}/\sqrt{\mathrm{mM}}$ (44).

Calcium-activated BK channel, I_{bk}

(*a*) The voltage-dependent parameters of the open probability P_{bk} are taken from ZhuGe et al. (22) and Wang and Mathers (45). BK channels are activated by cytoplasmic calcium, and are generally colocalized with calcium spark release channels (46). During the spark, BK channels are exposed to a mean calcium concentration of $\approx$10 μM, ~50–100 times the averaged $[Ca]_i$ (22). The sparking frequency P'_{bk} increased as a Boltzmann function of the potential V_m in the myogenic response range (23). The spark duration, τ, is 20–50 ms and does not depend on potential (22,46). We have changed the dependence of the sparking frequency on V_m into a dependence on $[Ca]_i$, based on the correspondence between calcium and membrane potential (10).

(*b*) The conductance g_{bk} was seeded at 0.6 nS (22,46).

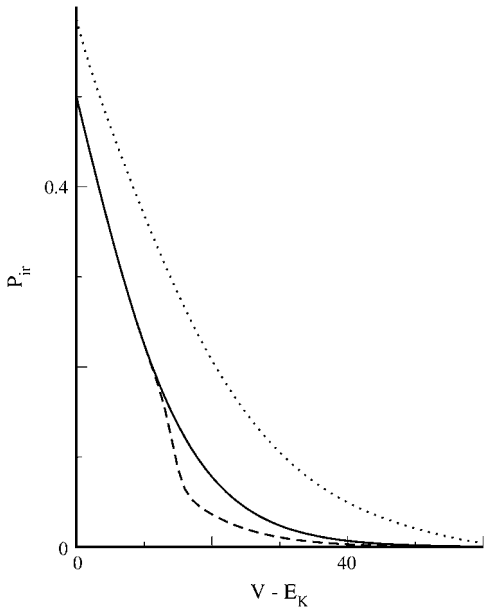

FIGURE 2 Open probability of the inward rectifier (IR) channel as a function of voltage. The solid line shows a Boltzmann function with an activation slope of 8.1 mV. The voltage plotted on the *x* axis is relative to the potassium reversal potential E_K; at these potentials, there is an outward current through the IR channel. These outward currents are not well-characterized in VSMCs. The probability in the model (in *dashed lines*) is slightly modified from the Boltzmann through a dip at ~15 mV positive to E_K. This change make the model stable at low pressures at an extracellular potassium concentration of 6 mM. Also plotted, in dotted lines, is the probability in the L-R model in cardiac myocytes (26).

Na-K pump, I_{NaK}

(*a*) We have used the formalism in the L-R model for cardiac myocytes (26,27,39). However, the Na and K half-saturation constants have been set to values reported for Na-K pumps in VSMCs (47).

(*b*) The maximal Na-K pump flux $\bar{I}_{NaK}$ was seeded to 20 pA (47). VSMCs have a capacitance of ~25 pF; the normalized value of 0.8 pA/pF may be compared to the corresponding value of 2.25 pA/pF in cardiac myocytes (39).

Background currents, $I_{b,c}$

(*a*) The background currents in vascular cells are not well characterized. We have used the formalism in Yang et al. (18).

(*b*) As the input resistance of smooth muscle cells is high, the leak conductances were set to low values: $g_{b,K} = 1.0$ pS, $g_{b,Ca} = 1.0$ pS, and $g_{b,Na} = 1.0$ pS.

Transmural pressure and stress on the membrane

In experiments on intact arteries, changes in intracellular calcium, voltage, and arterial diameter were measured against a range of transmural pressures from 10 to 100 mmHg (10). As we model only cellular and not tissue response in this work, we need to convert the applied transmural pressure, a tissue parameter, into a cellular parameter, namely membrane stress, which is the stimulus for the myogenic response (3,12,20,48). However, in these experiments, the myogenic response was such that the arterial diameter remained relatively unchanged over the range of applied pressures. According to Laplace's law, $\sigma/P = r/w$, where the radius r is ~60 μm, and the wall thickness w is ~15 μm. At constant diameter, this law implies that the stress σ varies linearly with pressure. We note that the stress σ as calculated by Laplace's law is the net wall stress in the vessel. However, we need to relate the wall stress to the membrane stress sensed by the stretch-sensitive channels. The total wall stress may be considered to be counterbalanced by two parallel components:

σ_e: Tension due to stretching (strain) of the passive extracellular matrix. A measure of the strain is provided by arterial diameter. Experimentally, this strain is only weakly altered by stress, since arterial diameter changes only slightly with transmural pressure when the vessel has myogenic tone. We therefore assume that σ_e does not change with pressure P.

σ_c: Tension due to intracellular components. This includes active force generation developed by myofibrils as well as passive forces from the cytoskeleton and the viscous cytoplasm. The change in net VSMC cell length is small with variations in transmural pressure, as VSMCs are circumferentially oriented; changes in cell length due to contraction of the force-generating elements would be counter-balanced by stretching of the passive cytoskeletal structures. As these intracellular components are connected in series, they would exert equal forces ($= \sigma_c$) in the steady state, where $\sigma_c = \sigma - \sigma_e$. It is likely that stretch-operated channels are coupled either to the cytoskeleton or to integrins (49), and that the stress that regulates their activity is σ_c. As noted before, we have followed (18) in modeling the dependence of the open probability on σ_c through a Boltzmann relationship.

The stress σ_e felt by the stress-sensitive channels differs from the wall stress $\sigma = (r/w)P$ only by the constant factor σ_e, which can be absorbed into the constant half-maximal tension parameter $\sigma_{1/2}$. We have used a conversion factor of 4 ($= r/w$) in converting from applied pressure to stress. A different conversion factor would not affect the results, though the stretch channel parameters $\sigma_{1/2}$ and k_σ would have to be appropriately rescaled.

Numerical methods

The equations in the Appendix were solved to satisfy the requirement that the fluxes for all three cations be zero in the steady state. This was achieved by varying V_m, $[Na]_i$, $[Ca]_i$, and $[K]_i$ for given external parameters, e.g., applied pressure or external ionic concentrations, subject to charge balance considerations. The variation was done such that the quantity Δ was minimized, where

$$\Delta^2 = (I_{Ca}^2 + I_K^2 + I_{Na}^2).$$

The symbol I_c refers to the total current carried by the cation c. The minimization was done using the simplex algorithm as implemented in the GNU scientific library. Standard extracellular ionic concentrations are given in Table 3, and these are used unless otherwise specified in the text. Seed values used for the minimization are listed in Table 4 for the state variables, V_m, $[Na]_i$, $[Ca]_i$, and $[K]_i$. Two seed values were tried for the membrane potential, due to the presence of dual bistable states in the model (see Results). Programs were written in C and compiled against the BLAS and GSL libraries.

Time dependence of currents

Although this article primarily deals with VSMCs in the steady-state, we have also done two time-dependent studies. In the first, we compute the instantaneous response to fast changes in some external condition, such as pharmacological block of the NaK pump. In calculating the instantaneous response, we assume that channel gating is fast and transient ionic currents do not have a major effect on $[Na]_i$ and $[K]_i$. Thus the membrane potential is the only variable parameter, and this is set to a value where all transmembrane ionic fluxes are zero.

In the second time-dependent simulation, we have compared the kinetics from experiment and model in response to changes in extracellular concentrations of $[Na]_o$ (see Alterations in $[Na]_o$, below). The transient response is calculated with the same adiabatic assumption that was used above when (say) the Na-K pump is blocked. That is, kinetics due to rapid channel gating is ignored, and all channels are assumed to have steady-state behavior appropriate to the current resting potential. Thus, only changes in intracellular ionic activity and membrane potential are followed with time. In all these kinetic simulations, we assume a 2-pL cell volume (50). We emphasize that any similarity in kinetics between experimental data and model is only indicative of compatibility.

RESULTS

We simulate five different experimental conditions below:

1. Pressurized arteries.
2. Na-K pump block.
3. Changes in $[K]_o$.
4. Channel block.
5. Changes in $[Na]_o$.

The results of the model are broadly in agreement with the experimental data.

TABLE 3 Standard ionic concentrations

Parameter	Definition	Value (mM)
$[K]_o$	Extracellular K concentration	6
$[Na]_o$	Extracellular Na concentration	140
$[Ca]_o$	Extracellular Ca concentration	2

TABLE 4 State variable initial conditions

Variable	Definition	Seed value for minimization (mM)
$[K]_i$	Intracellular K concentration	140 mM
$[Na]_i$	Intracellular Na concentration	6 mM
$[Ca]_i$	Intracellular Ca concentration	190 nM
V_m	Membrane potential	−80 or −50 mV

Estimation of parameters and justification

As discussed in Materials and Methods, values for intrinsic parameters, i.e., those parameters which describe the dependence of membrane currents on ionic concentrations, membrane potential, and $[Ca]_i$, are taken directly from the literature. However, for the stretch channel, the slope and half-maximum values of the Boltzmann dependence of current upon membrane tension are not experimentally characterized. Other variable (extrinsic) parameters are those that relate to the numbers of channels, pumps, and transporters, e.g., peak conductance and maximum pump current. There are thus a total of 10 variable parameters in the model (see Table 2). The seed values for these parameters were set as described in the individual subsections above in Materials and Methods for the channels and pumps.

Fig. 3, *A* and *B*, show the experimental data for $[Ca]_i$ and membrane potential V_m (as *solid squares*) (10). The experimental data covers six different applied transmural pressures from 10 to 100 mmHg (Fig. 6 in (10)). The model parameters were estimated by minimizing the difference between the predictions of the model (*solid lines*) and the experimental data on $[Ca]_i$ and V_m at these six transmural pressures.

In addition to the 10 variable parameters in the model, sodium and potassium concentrations ($[Na]_i$ and $[K]_i$) were also allowed to vary with applied pressure during minimization. These steady-state ionic concentrations are unchanged in the model if all the extrinsic parameters (maximum flux, peak conductance) are multiplied by a constant. One of them, namely the Na-K pump maximal flux ($\bar{I}_{NaK}$), was therefore fixed at 20 pA.

The final estimates for the variable parameters in the model are shown in Table 2. Almost all the parameter values are within a factor of 2 with respect to the seed values. One major difference between the seed and final values is in the LTCC conductance, g_l. There are two explanations for this difference:

1. The current from this channel is small.
2. The dependence of its inactivation on V_m has a relatively long time constant (seconds), and is not well-characterized experimentally.

The estimate of the maximal flux across the NCX also differs from the seed value. However, this is perhaps not significant given that the seed value was chosen somewhat arbitrarily in the absence of relevant experimental data.

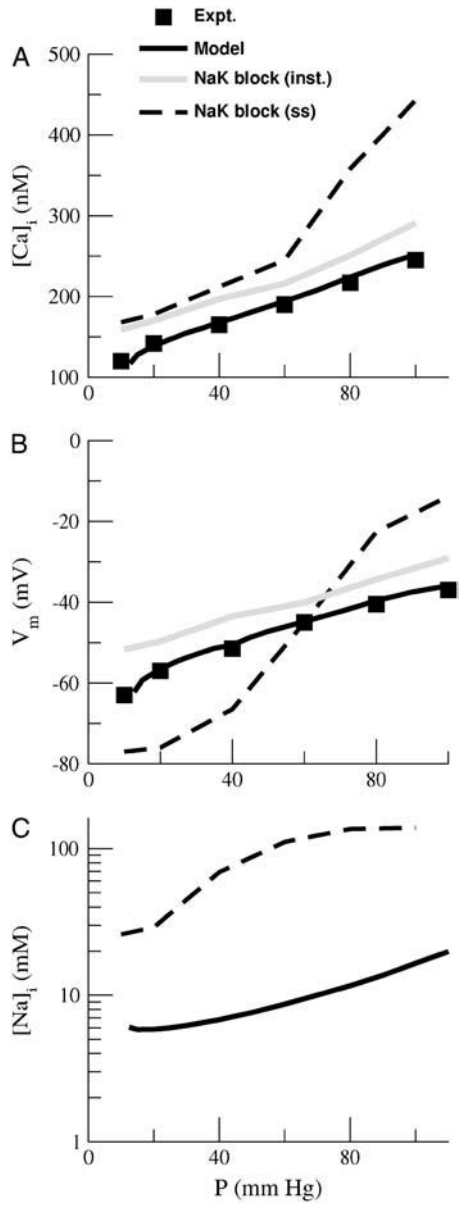

FIGURE 3 Steady-state $[Ca]_i$, V_m, and $[Na]_i$ over the range of intravascular pressures. The three panels, from top to bottom, show $[Ca]_i$, membrane potential V_m, and $[Na]_i$, respectively, in the steady state over a range of transmural pressures. The results for $[Ca]_i$ and V_m from the model (*solid black lines*) are compared with experimental data (*solid squares*) from Figs. 5 and 7 *A* in Knot and Nelson (10). In the model, $[Na]_i$ increases threefold during the elevation of pressure from 10 mmHg to 100 mmHg. This increase is necessary to activate the Na-K pump, which counterbalances pressure-induced sodium flux from stretch channels. The solid gray and dashed black lines represent instantaneous (*inst*) and steady-state (*ss*) values when the Na-K pump is blocked; instantaneous values for $[Ca]_i$ and V_m are calculated by fixing $[Na]_i$ at its steady-state value when the pump is not blocked (please see text for details). Blocking the pump results in immediate depolarization and increase in $[Ca]_i$; at low pressures, the cells eventually hyperpolarize.

There are two parameters describing the Boltzmann response of the stretch channel to membrane tension—the slope k_σ and the half-maximum tension $\sigma_{1/2}$. The value for the slope k_σ corresponds to a transmural pressure of 27 mmHg, which is approximately half the isobaric pressure (60 mmHg). However, the transmural pressure corresponding to the tension where the channel is half-maximally activated is 137 mmHg, which is more than twice the isobaric pressure. The current through the stretch channel would thus almost linearly increase with membrane tension (or pressure) in physiological conditions. In fact, this accords with experimental data where the open probability P_m of the channel is a linear function of the applied stress (30).

Sodium as a function of applied pressure

Fig. 3 *C* shows the variation predicted by the model in $[Na]_i$ with pressure (in *solid lines*); $[Na]_i$ changed from 5.93 mM at low pressures (10 mmHg) to 16.92 mM at high pressures (100 mmHg). The sodium concentration of 8.56 mM in the model at a transmural pressure of 60 mM Hg is comparable to experimentally observed basal values of 10–11 mM (51–53). The rise of $[Na]_i$ with increasing transmural pressure is an experimentally testable prediction of the model. It may be noted that ventricular myocyte models (26,27) exhibit similar changes in $[Na]_i$ if it is clamped at a depolarized state (data not shown).

Individual currents

Fig. 4, *A–C*, shows the contributions of the calcium, potassium, and sodium fluxes in the model over a range of transmural pressures. It may be noted that the fluxes through the Na-Ca exchanger (NCX) in the forward mode are relatively small in comparison to other fluxes for both sodium and calcium. The relative contribution of the inward rectifier to K^+ flux as compared to the other three potassium channels is higher at small applied pressures ($\leq$40 mmHg) (54); this is explored in detail below (please see Bistable States). Overall, $[Ca]_i$ and V_m vary with transmural pressure in a manner such that ionic fluxes have an almost linear dependence on pressure.

Blocking the Na-K pump

Fig. 3 also shows the effects of blocking the Na-K pump on $[Ca]_i$, membrane potential, and $[Na]_i$. The dashed lines in these panels show the response in the steady state, which is achieved in times of an hour or more at high transmural pressures (see also Fig. 9 *B*). $[Na]_i$ values in the steady state vary from 26 mM at low pressures (10 mmHg) to 139 mM (100 mmHg). This range is comparable to the 25 mM observed in unstretched smooth muscle strips after 1 h of application of ouabain (52), 65 mM in an isometrically stretched vascular preparation after 1 h (51), or an increase of 6.3 mM in 10 min in cultured VSMCs after ouabain-induced block (53).

Fig. 4 *C* shows the sodium flux through the NCX when the Na-K pump is blocked (*dashed line*). As has been noted (52),

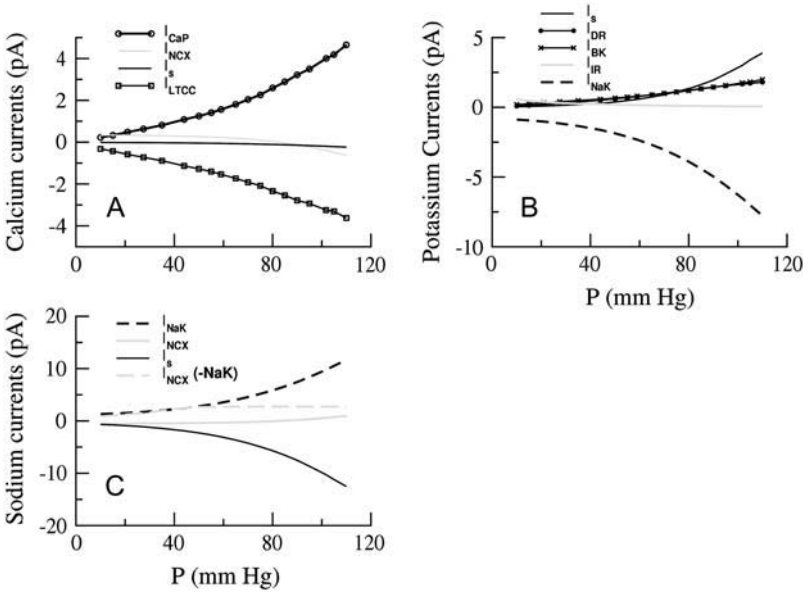

FIGURE 4 Channel, pump, and transporter currents as a function of transmural pressure. Panels *A*, *B*, and *C* show calcium, potassium, and sodium currents, respectively, as a function of transmural pressure. Calcium fluxes are dominated by outward flux through the calcium pump (I_{CaP}) and inward flux across L-type calcium channels I_l. Calcium flux across the sodium-calcium exchanger I_{NCX} is small under physiological conditions. Potassium influx (*B*) is driven by the Na-K pump I_{NaK}. There is comparable efflux across the two voltage-sensitive potassium channels— the delayed rectifier I_{dr} and the calcium-sensitive large potassium channel I_{bk}. Potassium efflux I_{ir} across the inward rectifier is significant relative to other fluxes only at low pressures. Pressure-activated sodium influx across the stretch channel $I_{s,\,Na}$ is balanced by sodium efflux driven by the Na-K pump, which is activated by increasing $[Na]_i$ at high transmural pressures. The dashed gray line in panel *C* shows the sodium flux across the sodium calcium exchanger (NCX) when the Na-K pump is blocked. In its reverse mode of operation, the NCX can compensate for the blocked Na-K pump at low transmural pressures. At pressures >40 mmHg, the intracellular sodium concentration approaches extracellular levels (*bottom panel* of Fig. 2), and flux across the NCX saturates.

the relatively small increase in $[Na]_i$ at low transmural pressures (to 26 mM at 10 mmHg) after Na-K pump block is due to NCX reverse-mode activity. However, the model predicts that the membrane potential would be hyperpolarized. This may seem counterintuitive, since the Na-K pump is electrogenic, and blocking the pump should apparently depolarize the membrane. Nevertheless, the prediction of a hyperpolarization at low pressures upon Na-K pump blockade is a testable prediction of the model.

It should be noted that the predicted hyperpolarization at low pressures would be observed only in the steady state. Fig. 3, *A* and *B*, also show the instantaneous response after block of the Na-K pump in gray lines. It may be seen that the membrane depolarizes almost uniformly by ~6–7 mV over the entire range of transmural pressures, while $[Ca]_i$ also increases uniformly by ~30–50 nM. These results are compatible with the 17 nM immediate increase in $[Ca]_i$ observed in isolated detrusor cells (55) upon blocking the Na-K pump with strophanthidin (100 μM).

In isometrically stretched mesenteric vessels, 1 mM ouabain reduced sodium efflux by approximately half (51). The model predicts a similar reduction in sodium efflux, upon Na-K pump block, at ~70 mmHg transmural pressure (Fig. 4 *C*).

Bistable states

Two stable states exist in the model over a range of transmural pressures. Fig. 5 shows these two states, which we label as the upper and lower states, as solid and dashed lines, respectively; $[K]_o$ was set to 4.8 mM. In the pressure range of 0–35 mmHg where both states coexist, the lower state is hyperpolarized by ~15–17 mV with respect to the upper state and $[Ca]_i$ differs by ~50–70 nM. The bistable behavior of the model at low pressures appears to be qualitatively consistent with observations in unstretched strips from the spiral modiolar artery (56). In this preparation, the resting potentials had a bimodal distribution, with two stable levels at ~−40 and −75 mV. These were, arespectively, labeled low-RP and high-RP states.

Fig. 6 shows the unfolding of the two stable states as external $[K]_o$ is varied from 1.5 mM to 15 mM. The range of pressures over which the two states coexist reduces with increasing $[K]_o$, with an overlap of almost zero when $[K]_o$ is 15 mM. These dual stable states arise in the model due to the bell-shape of outward currents through the IR channel (Fig. 2). Fig. 6 *C* shows steady-state $[Ca]_i$ (in *dotted lines*) when I_{ir} is set to zero in the model; it can be seen that the lower state disappears. Two pieces of experimental evidence support this interpretation:

1. In unpressurized spinal arteries ($[K]_o$ = 4.8 mM), a cell in a high-RP state could be shifted to the low-RP state by a brief application of barium, a blocker of IR channels (56); and
2. In renal afferent arterioles (54), blocking the IR channel with barium causes a leftward shift in the activation curve of tone with pressure. The relaxed diameter of renal arterial vessels (18 μm) is substantially smaller than that of cerebral resistance arteries (100 μm); nevertheless, the results of the model upon IR channel block agree qualitatively with the experimental data.

The model also offers a possible explanation for the experimentally observed differences in graded versus nongraded response upon stepwise changes in pressure (10,57)

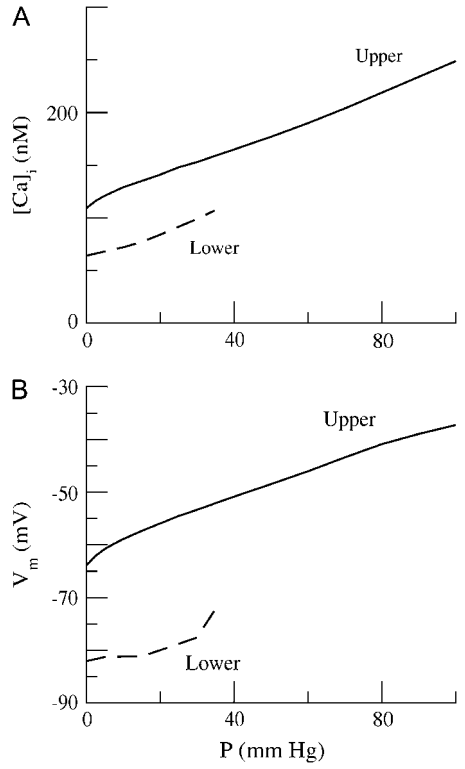

FIGURE 5 Two stable states coexist at $[K]_o = 4.8$ mM. Panels *A* and *B* show steady-state $[Ca]_i$ and V_m as a function of transmural pressure at an extracellular potassium concentration $[K]_o$ of 4.8 mM. The two lines in both graphs reflect the existence of two stable states in the model. These states can coexist over a range of pressures, from 0 to ~35 mmHg. At higher pressures, only one state (the upper state) is stable. $[Ca]_i$ differs by 60–70 nM and V_m by ~15 mV between these two states. Coexisting dual stable states are made possible by the bell-shape of outward currents through the inward rectifier as a function of membrane potential (please see text for details).

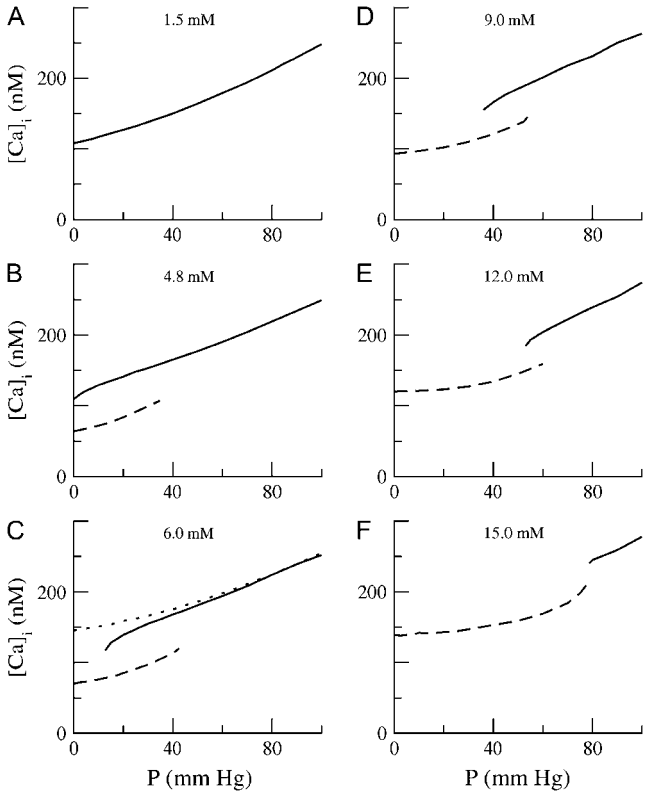

FIGURE 6 Varying $[K]_o$ from 1.5 to 15 mM affects the two stable states differently. At very low $[K]_o$, there is one stable state, the upper state (*solid line* in *all panels*). At $[K]_o = 4.8$ mM, an alternate stable state emerges, the lower state, which is stable only at low pressures (*dashed line* in *all panels*). With increasing $[K]_o$, the upper state become destabilized at low pressures, even while the range of pressures over which the lower state is stable, increases. The range of pressures over which the two states can coexist also decreases with increasing $[K]_o$, becoming close to zero at $[K]_o = 15$ mM. Outward potassium currents in the lower state are dominated by the inward rectifier (IR) channel, while other potassium channels play a major role in the upper state. The dotted line in the panel for $[K]_o = 4.8$ mM is the only stable state when the IR channel is blocked. This state is depolarized even with respect to the stable state, and exhibits higher $[Ca]_i$ at low pressures.

at $[K]_o = 6$ mM (Fig. 6 *C*). In the experimental protocol followed in Knot and Nelson (10), the arteries were equilibrated at 60 mmHg, where only the upper state is stable. It is possible that these arteries remained in the upper state as pressure was changed, resulting in a graded depolarization at lower pressures. In the protocol in Osol et al. (57), the arteries were equilibrated at 10 mmHg, where only the lower state is stable. As pressure is increased beyond 45 mmHg, the lower state is destabilized in the model and the system would shift abruptly to the upper state. This behavior seems to mimic the experimental observations (57), where calcium increases suddenly as the transmural pressure is increased from 50 to 60 mmHg.

Fig. 7 plots the potential V_m as a function of $[Ca]_i$ for all values of $[K]_o$ shown in Fig. 6. Values from the upper state are plotted as open circles, and values for the lower state as solid circles. The points from both upper and lower curves are similar where there is an overlap, in the range of potentials from -60 mV to -30 mV. This implies that changes in $[K]_o$, or pressure, do not change the dependence of $[Ca]_i$ on V_m, as has been noted (10).

In a common experimental protocol, pressurized cannulated arteries are exposed to increasing $[K]_o$ in a stepwise fashion (10,54,58). Under these conditions, the artery dilates at some $[K]_o$ ranging from 7 to 10 mM, and this response is usually not graded with $[K]_o$. The abrupt dilation is accompanied by a hyperpolarization and a decrease in $[Ca]_i$. This experimental scenario is akin to taking a cross-section at a fixed pressure across the panels in Fig. 6. Fig. 8 shows this cross section for both upper and lower stable states at a transmural pressure of 60 mmHg (in *solid lines*), along with experimental data from Knot and Nelson (10) (as *solid squares*). While the model qualitatively mimics the behavior and shape of the experimental data, it can be seen from Fig. 8 that the predicted hyperpolarization and change in $[Ca]_i$ are less than that observed.

In renal afferent arterioles (54), a step change of $[K]_o$ from 5 mM to 1.5 mM induced vasoconstriction at low pressures

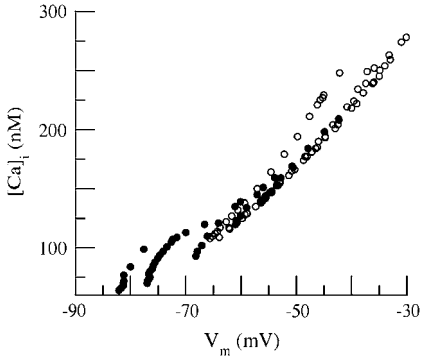

FIGURE 7 $[Ca]_i$ is a function of the membrane potential V_m. $[Ca]_i$ is plotted against V_m for all values of $[K]_o$ in Fig. 6. Points corresponding to the lower and upper states in Fig. 6 are plotted as solid and open circles, respectively. There is reasonable overlap between points from both states. Overall, $[Ca]_i$ depends only on the membrane potential V_m over a range of pressures and $[K]_o$.

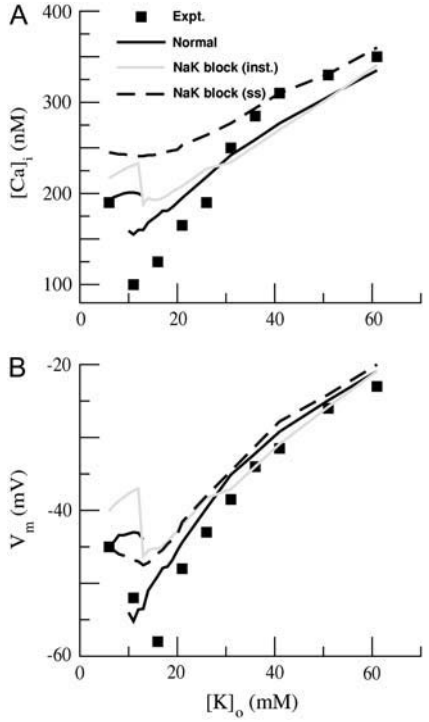

FIGURE 8 Biphasic effect of $[K]_o$ on $[Ca]_i$ and V_m at a fixed transmural pressure. Panels *A* and *B* show $[Ca]_i$ and V_m, respectively, as a function of ($[K]_o$) at a fixed transmural pressure of 60 mmHg, in solid black lines. At this pressure, the system is in the upper stable state at $[K]_o = 6$ mM (see Fig. 6 *C*). As $[K]_o$) is increased to 9 mM (Fig. 6 *D*), both upper and lower states become stable at a pressure of 60 mmHg. At an even higher $[K]_o$ of 12 mM, the upper state becomes unstable, and the system has to transit in a nongraded manner to the lower state. $[Ca]_i$ and V_m in the lower state increase smoothly with further increases in $[K]_o$. Experimental data (10) is plotted as solid squares; the changes in $[Ca]_i$ in the data are greater than seen in the model. Blocking the Na-K pump preserves the nongraded nature of the response immediately after the block (*gray lines*). Once steady state is achieved after Na-K pump block, the response (*dashed black lines*) become graded with increasing $[K]_o$, though a small hyperpolarization and reduction in $[Ca]_i$ is still seen at $[K]_o = 12$ mM.

and vasorelaxation at high pressures. In Fig. 6, the panels *A* and *B* for steady-state $[Ca]_i$, when $[K]_o$ is 1.5 mM and 4.8 mM, respectively, may be compared. The lower state disappears at low $[K]_o$, implying that reduction in $[K]_o$ at low pressures would cause the system to move from the lower to the upper state, inducing depolarization and an increase in $[Ca]_i$ (by ~50 nM). At high pressures (>40 mmHg), in the model, the system remains on the upper state as $[K]_o$ is lowered to 1.5 mM; the upper state itself hyperpolarizes by ~5 mV, and there is a small decrease in $[Ca]_i$. The model is thus qualitatively consistent with the experimental observations reported in Chilton and Loutzenhiser (54).

Nongraded dilation upon increased $[K]_o$ is also seen experimentally when the Na-K pump is blocked by ouabain (0.1 mM) (58). In the model, as shown in Fig. 8 in dashed black lines, blocking the Na-K pump results in a graded response in $[Ca]_i$ upon $[K]_o$ increase. However, the instantaneous behavior of the model (*gray lines*) shows nongraded behavior. Moreover, increasing the ouabain concentration (to 0.5 mM) abruptly reversed the $[K]_o$ induced dilation in cerebral arteries (58), implying that Na-K pump block was only partial at the lower ouabain dose (of 0.1 mM). With partial block of the Na-K pump, the model exhibits dual stable states, with an abrupt reduction in $[Ca]_i$ as $[K]_o$ is increased (data not shown).

The model predicts an increase in $[Na]_i$ when the artery is abruptly relaxed by increasing $[K]_o$. This is an experimentally testable consequence of the model. At a transmural pressure of 60 mmHg and with $[K]_o$ at 12 mM, for instance, steady-state $[Na]_i$ values in upper and lower states are 7.3 and 9.4 mM, respectively. The model also predicts a lowering of $[Na]_i$ as $[K]_o$ is further increased; for example, changing $[K]_o$ from 16 to 61 mM reduces $[Na]_i$ from 7.6 to 3.0 mM.

As noted in Materials and Methods, we have assumed that membrane stress is directly proportional to transmural pressure. This was predicated on the observation (Fig. 6 *b* of (10)) that arterial diameter is fairly constant at 120 μm for transmural pressures from 10 to 100 mmHg. However, as alterations in $[K]_o$ do change arterial diameter, all of the results shown here for a single smooth muscle cell may not be directly applicable to the intact vessel. A complete mechano-electro-chemical model would be needed to address this issue; it is considered further in Discussion, below.

Effect of channel blockers

Table 5 compares experimental data and model results for $[Ca]_i$ and V_m from pressurized arteries when various channels are blocked pharmacologically. The experimental data derive from observations in cerebral arteries (7,10,42,59). The majority of the experimental results relate only to V_m; the $[Ca]_i$ data, where available, is shown in parentheses in Table

5. The results from the model considered here hold for cannulated arteries only under the assumption of constant arterial diameter, while many channel blockers, especially those for LTCCs, change arterial diameter drastically. Thus any similarity between the model results and the experimental data can be seen only as indicative.

Overall, there is reasonable agreement between the trends in the model and the experimental data. In many cases, there is also quantitative agreement between data and model. However, there are two major exceptions:

1. Blockers of the DR channel, namely 4-AP (1 mM) and 3,4-DAP (1 mM), depolarized cerebral arteries by 19 and 21 mV, respectively, at a transmural pressure of 80 mmHg (59). The depolarization in the model with DR channel block was only 6 mV, with $[Ca]_i$ increasing from 223 to 252 nM. This is a major difference between the model and the experimental data. However, blocking DR and BK channels simultaneously in the model depolarized the cell by 23 mV, comparable to the experimental data.
2. Model and experimental results are similar if either LTCC or BK channels are blocked. However, arteries experimentally do not depolarize when LTCCs and BK channels are blocked simultaneously (at 80 mmHg), whereas the model predicts a depolarization of 6 mV.

Alterations in $[Na]_o$

A reduction in extracellular sodium affects the model in three ways: 1), the voltage-dependence of the Na-K pump is reduced (60); 2), the reverse-mode activity of the NCX is increased (37), with a Hill coefficient of 2 and a K_d of 60 mM (40); and 3), the stretch-activated sodium influx is lowered due to the shift in sodium reversal potential. At very low $[Na]_o$ (below 10 mM), the sodium flux across the stretch channel is so small that the cell becomes unresponsive to pressure.

TABLE 5 Comparison of membrane potential and intracellular calcium from experimental data and the model, under channel block

	Pressure			
	60 mmHg		80 mmHg	
	Data	Model	Data	Model
PSS	−45 (197)	−44.8 (194)	−40	−39.8 (223)
PSS/NISOL	−45 (80)	−44.8 (107)	−38	−38.8 (130)
PSS/IbTX	−35 (248)	−39.1 (220)	−31	−33.7 (253)
PSS/DILT/IbTX			−38	−34.4 (126)
PSS/4-AP			−21	−33.9 (252)
PSS/4-AP/NISOL			−24	−29.9 (122)
PSS/4-AP/IbTX			−18	−17.0 (368)
PSS/4-AP/DILT/IbTX			−21	−18.7 (115)

The results from the model when various channels are blocked are compared to experimental data from the literature (7,10,42,59). The membrane potential V_m is shown along with values for $[Ca]_i$ in parentheses, where known. *PSS* stands for the normal extracellular saline (140 mM NaCl, 6 mM KCl, and 2 mM $CaCl_2$). Nisoldipine (NISOL) or diltiazem (DILT) block LTCC channels, iberiotoxin (IbTX) blocks BK channels, and 4-aminopyridine (4-AP) blocks delayed rectifier channels.

The solid line in Fig. 9 *A* shows $[Ca]_i$ as a function of time (with the adiabatic assumption) when $[Na]_o$ is suddenly lowered to 5 mM at $t = 0$. In this simulation, $[K]_o$ was set to 4.7 mM. There is a small increase in $[Ca]_i$ (~25 nM) that persists in the steady state. These results are in accord with experimental data in aortic VSMCs (61). Fig. 9 *A* also shows the response (*dashed line*) when the Na-K pump is first blocked, and the cell is subsequently challenged by abruptly lowering $[Na]_o$ to 5 mM at $t = 0$. As noted earlier, blocking the Na-K pump itself increases baseline $[Ca]_i$. With lowered $[Na]_o$, $[Ca]_i$ is transiently increased by ~200 mM, and is elevated by 26 nM after 10 min. This compares with the experimental data, after block of calcium release from the SR (Fig. 8 in (61)), where $[Ca]_i$ transiently increased by 120 nM, and remains elevated after 10 min by 26 nM. It should be noted that experimental responses are very different when the SR release is not blocked, and there seems to be some indication of a secondary phenomenon that increases $[Ca]_i$ again after 7–8 min.

The forward-mode activity of the NCX was evaluated in Batlle et al. 61) by testing the effect of ionomycin on aortic VSMCs. We simulated this effect by increasing background calcium channel activity by a factor of 7.5, when basal $[Ca]_i$ increased by 100 nM, comparable to the data (Fig. 10 in (61)). Lowering $[Na]_o$ in the presence of ionomycin transiently increased model $[Ca]_i$ by 140 nM; steady-state $[Ca]_i$ was 123 nM above basal level. In the experimental data (Fig. 11 in (61)), increases in $[Ca]_i$ with nominally zero $[Na]_o$ were much higher, ~350 nM transiently, and 150 nM in the steady state. As noted above, the difference between model and experiment may arise partly from transient SR fluxes and a secondary calcium-influx component, both of which are not taken into account in the model.

Fig. 9 *B* shows the results of simulations obtained under a different protocol (51,52), where the Na-K pump was blocked at $t = 0$ ($[K]_o = 6$ mM). Blocking the Na-K pump results in a gradual increase in $[Na]_i$ (*dashed line* in Fig. 9 *B*). Also plotted in Fig. 9 *B* (*solid line*) is the peak of the transient increase in calcium upon brief application of 5 mM $[Na]_o$. The relationship between $[Ca]_i$ and $[Na]_i$ in this protocol is almost linear, which may correlate to the observed linearity between $[Na]_i$ and force (52).

Fig. 9 *C* shows the change in $[Ca]_i$ when the cell is challenged briefly by various $[Na]_o$ after a steady state has been reached with Na-K pump block. The shape of the curve is similar to the observed-force $[Na]_o$ with this protocol (panels *B* and *C* of Fig. 9 may be compared with panels *b* and *c* of Fig. 1 in (51)).

The results from the simulations at low $[Na]_o$ do not agree with several experimental observations:

Reducing $[Na]_o$ to nominally zero has no effect on resting membrane potential or arterial diameter in cerebral

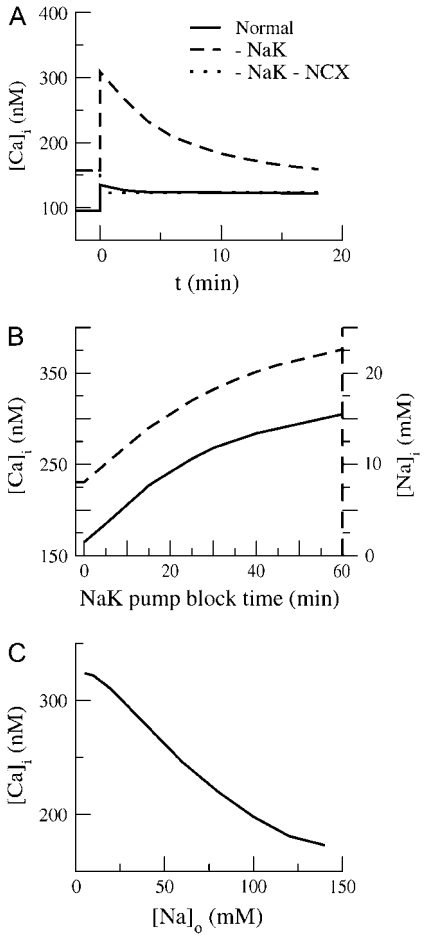

FIGURE 9 Lowering $[Na]_o$ increases $[Ca]_i$. This figure shows the effect of lowered $[Na]_o$ on isolated cells. In panel *A*, $[Na]_o$ was suddenly lowered to 5 mM, 1), after steady state had been achieved at zero pressure (*solid line*); 2), under Na-K pump block (*dashed line*); and 3), while both the Na-K pump and the NCX were blocked (*dotted line*). There is a small elevation of $[Ca]_i$, ~25 nM, under normal conditions and under dual block. When the Na-K pump alone is blocked, there is a sharp transient increase in $[Ca]_i$ due to the reverse-mode activity of the NCX. The magnitude of the response is comparable to that seen in experimental data (61). $[Ca]_i$ gradually decreases as intracellular sodium concentration $[Na]_i$ decreases below extracellular levels. Panel *B* shows the peak of the transient $[Ca]_i$ response of cells to a brief lowering of $[Na]_o$ (to 5 mM) at various times after block of the Na-K pump. $[Na]_i$ gradually increases (*dashed line*) with time, and this increase correlates to larger $[Ca]_i$ transient peaks, as mediated by the NCX. Panel *C* shows the peak of the transient $[Ca]_i$ response as a function of $[Na]_o$ as the steady state is reached after block of the Na-K pump. The magnitude of the response is potentiated as $[Na]_o$ is lowered. The results from the model, as shown in panels *B* and *C*, correlate with the trends in the experimental data (51).

arteries pressurized to 80 mmHg (62). In the model, at zero $[Na]_o$, the cell hyperpolarizes to values close to the potassium reversal potential.

The data from skeletal muscle arterioles (63,64) indicate a large constriction when extracellular sodium is lowered, which is not seen in the model.

In skeletal muscle arterioles (63), inhibiting NCX activity with KB-R7943 hyperpolarized the membrane from −35 mV to −43 mV with an accompanying large vasodilation, at 80 mmHg. In the model, under these conditions, the hyperpolarization was 1 mV, and intracellular calcium levels remained unchanged.

Large changes (70 nM) in $[Ca]_i$ were also observed in isolated detrusor smooth muscle cells (55) upon decreasing $[Na]_o$ from 140 to 30 mM. The changes in the model were much smaller (20 nM); this difference may be attributable to calcium release from the SR, as has been noted above.

DISCUSSION

In this study, we have formulated an electrochemical model for myogenic tone in VSMCs, which incorporates membrane channels and transporters. The results of the model are consistent with data obtained under three experimental conditions:

1. Changes in applied pressure.
2. Block of channels, pumps, and transporters by pharmacological treatments.
3. Variation in external K or Na concentrations.

The magnitude of the macroscopic conductances of the channels and the maximum flux through the various pumps and transporters are comparable to estimates in the literature (see Table 2). The resulting currents are of the order of pA, and are consistent with the high input resistances ($\geq$10 $G\Omega$) characteristic of vascular smooth muscle cells. The various intrinsic parameters (such as potential activation slopes, half-activation voltages, or calcium dependence) were either fixed directly from previous estimates in VSMCs or were taken from parameters in ventricular cell models (26,27,39).

The only significant change in an intrinsic parameter in the present model is the introduction of small changes in the description of outward currents across the IR channel. As these outward currents are rather small in VSMCs, they are not well-characterized experimentally; yet they play a significant role both in setting the resting membrane potential as well as in responses to changes in $[K]_o$. In the model, the open probability of IR channels at potentials >15 mV positive to E_K is reduced compared to a Boltzmann distribution. This change shifted the appearance of the lower state in the model to higher $[K]_o$, and made the model results more compatible with the experimental data at a $[K]_o$ of 6 mM (7,10). It may be that the outward IR currents are best characterized by optimizing for fits between experimental data and model results at various $[K]_o$ values, although this would have to be done in the context of a complete mechano-electro-chemical model of the arterial wall.

The model does not include contributions from anion channels, such as the Ca-dependent chloride channels that have been documented in arteries elsewhere (65). These may play a role in setting myogenic tone in some tissues (23, 66). We have also not included an explicit contribution for the K-ATP channel. However, this channel, which is

voltage-independent (67), is believed to be characterized in a manner very similar to the K background current.

As noted earlier, the work of Yang et al. (18,19) is the only previous model of electrochemical processes in VSMCs. The model in Yang et al. (18,19) differs from the model considered here in some key aspects:

- The model in Yang et al. (18,19) concentrated primarily on fast kinetics in VSMCs, where slow processes such as the inactivation of the LTCC do not play a major role. However, slow processes are significant in the steady state.
- Additionally, the model in Yang et al. (18,19) did not consider the calcium-dependence of maxi-K channels through calcium sparks. Maxi-K activation by $[Ca]_i$ plays an important role in setting steady-state $[Ca]_i$.
- A further complication is added by the difficulty created when extrinsic parameters, i.e., those describing the peak channel conductances or maximal pump fluxes, are directly set to values in the literature, as was done in Yang et al. (18,19). While this is perhaps not significant in fast kinetic models, extrinsic parameters cannot be set independently in steady-state models, where all transmembrane fluxes are constrained to be zero over a range of transmural pressures. In the present model, we have adjusted the values of extrinsic parameters to satisfy this constraint. It is likely that the factors noted above played a role in improving the agreement between the results from the current model and steady-state experimental data.

The contributions of the various model components are shown In Fig. 3, and have been briefly discussed in Individual Currents, above. Some additional points are:

- For transmural pressures >40 mmHg, the contributions from the three potassium channels (I_{bk}, I_{dr}, and $I_{s,K}$) are similar over the range of transmural pressures. In fact, the dependence of I_{bk} on calcium and I_{dr} on voltage is similar enough for each to replace the other under physiological conditions. It is possible that their different roles manifest themselves only in the kinetics of the myogenic response.
- The NCX does not play a significant role in physiological conditions (Fig. 3). However, the simulations above show that the NCX plays a stabilizing role in maintaining myogenic tone under conditions where the NaK pump is blocked or there is a moderate decrease in external Na.

An interesting prediction of the model is the existence of dual stable states under a variety of external conditions. The existence of these states followed from the bell-shape of outward currents through the IR channel. When these states coexist, they are marked by different $[Ca]_i$ and V_m. This implies that the response of the cell would be nongraded when the system makes a transit from one to the other of these states in response to changes in external conditions, such as changes in pressure, external [K], or IR block. This qualitative prediction of a nongraded behavior agrees with experimental data (10,54,58).

The results of the model indicate that, in many experimental conditions, VSMC responses are accompanied by changes in intracellular [Na]. For example, intracellular [Na] in the model varies greater than threefold with a transmural pressure increase from 10 to 100 mmHg. Other experimental manipulations, such as blocking the Na-K pump and variation in external [K] and [Na], also affect $[Na]_i$, as noted in Results, above. $[Na]_i$ also differs across coexisting stable states, and changes in $[Na]_i$ should be co-observable with nongraded cell responses in the steady state. It would appear that monitoring of $[Na]_i$, simultaneously with $[Ca]_i$ and V_m, would be a useful tool in refining cellular models.

In this article, we have presented a basic model for steady-state electrochemical behavior in VSMCs. The results of the model broadly agree with experimental data under a variety of external conditions. The model can serve as a basis for more elaborate models, e.g., to predict time-dependent transients by including channel kinetics and calcium buffering. Again, the inclusion of downstream effects of changes in $[Ca]_i$, such as muscle tension, as well as tension from passive extracellular components, would allow for a complete model that can be used to predict changes in arterial diameter with pressure.

APPENDIX: MEMBRANE CURRENTS

Voltage-operated L-type calcium channel, I_l

$$I_l = g_l d_l f_l b_l (V_m - E_{Ca}), \tag{1}$$

$$d_l = \frac{1}{1 + e^{-(V_m - 6.2)/9.5}}, \tag{2}$$

$$f_l = 0.74\bar{f_l} + 0.26, \tag{3}$$

$$\bar{f_l} = \frac{1}{1 + e^{(V_m + 24.2)/9.6}}, \tag{4}$$

$$b_l = \frac{1}{1 + (Ca_i/6 \times 10^{-4})^2}, \tag{5}$$

$$E_{Ca} = (RT/2F)\ln([Ca]_o/[Ca]_i). \tag{6}$$

Stretch-operated channels, $I_{s,c}$

$$I_{s,c} = g_s P_m \rho_c z_c v_m \frac{[c]_o - [c]_i e^{v_m}}{1 - e^{v_m}};\ c = \text{K, Na, or Ca}, \tag{7}$$

$$P_m = 1/(1 + e^{-(\sigma - \sigma_{1/2})/k_\sigma});\ v_m = (F/RT) z_c V_m, \tag{8}$$

$$\rho_K : \rho_{Na} : \rho_{Ca} = 3 : 2 : 1. \tag{9}$$

Calcium extrusion pump, I_{cp} or I_{CaP}

$$I_{cp} = I_{0,cp}\frac{[Ca]_i^4}{[Ca]_i^4+(k_{cp})^4}. \quad (10)$$

Sodium calcium exchanger, I_{NCX}

$$I_{NCX} = \bar{I}_{NCX}\, r\, e^{(\gamma-1)V_mF/RT} \quad (11)$$

$$\times \frac{e^{V_mF/RT}[Na]_i^{3.0}[Ca]_o - [Na]_o^{3.0}[Ca]_i}{1+C_2e^{(\gamma-1)V_mF/RT}(e^{V_mF/RT}[Na]_i^{3.0}[Ca]_o + [Na]_o^{3.0}[Ca]_i)}, \quad (12)$$

$$C_2 = 10^{-4}\,(mM)^{-4};\ \gamma = 0.15, \quad (13)$$

$$r = 1;\ I_{NCX} \geq 0, \quad (14)$$

$$r = \frac{6.44}{1+(Na_o/60)^2};\ I_{NCX} < 0. \quad (15)$$

Delayed rectifier channel, I_{dr}

$$I_{dr} = g_{dr}P_{dr}(V_m - E_K), \quad (16)$$

$$P_{dr} = \frac{1}{1+e^{-(V_m+2.0)/9.57}}\frac{1}{1+e^{(V_m+34.7)/7.0}}, \quad (17)$$

$$E_K = (RT/F)\ln([K]_o/[K]_i). \quad (18)$$

Inward rectifier channel, I_{ir}

$$I_{ir} = g_{ir}P_{ir}(V_m - E_K), \quad (19)$$

$$g_{ir} = G_{ir}[K]_o^{0.5};\ P_{ir} = p_{ir}\theta, \quad (20)$$

$$p_{ir} = 1/\{1+e^{-(V_m-V_{1/2})/8.1)}\}, \quad (21)$$

$$\theta = \alpha_1/(\alpha_1+\beta_1);\ \alpha_1 = 1/\{1+e^{0.06(V_m-E_K-200)}\}, \quad (22)$$

$$\beta_1 = \frac{e^{0.0002(V_m-E_K+100)}+0.1e^{0.03(V_m-E_K-15)}}{1+e^{-1.3(V_m-E_K-15)}}. \quad (23)$$

Calcium-activated BK channel, I_{bk}

$$I_{bk} = g_{bk}\tau P'_{bk}P_{bk}(V_m - E_k), \quad (24)$$

$$P_{bk} = 1/\{1+e^{-(V_m+40.0)/(21.0)}\}, \quad (25)$$

$$P'_{bk} = 0.3+0.7/\{1+e^{-(Ca_i-2.79\times10^{-4})/(4.2\times10^{-5})}\}, \quad (26)$$

$$\tau = 0.050\,s. \quad (27)$$

Na-K pump, I_{NaK}

$$I_{NaK} = \bar{I}_{NaK}f_{NaK}\frac{[Na]_i^{1.7}}{[Na]_i^{1.7}+(k_{Na})^{1.7}}\frac{[K]_o^{1.1}}{[K]_o^{1.1}+(k_K)^{1.1}}, \quad (28)$$

$$f_{NaK} = [1+0.1245\exp(-0.1\,V_mF/RT) + 0.219\,\alpha_2\exp(-V_mF/RT)]^{-1}, \quad (29)$$

$$\alpha_2 = (1/7)[\exp([Na]_o/(67.3)-1], \quad (30)$$

$$k_{Na} = 22\,mM;\ k_K = 1.6\,mM. \quad (31)$$

Background currents, $I_{b,c}$

$$I_{b,c} = g_{b,c}(V_m - E_c),\ c = K,\ Na,\ or\ Ca, \quad (32)$$

$$E_{Na} = (RT/F)\ln([Na]_o/[Na]_i). \quad (33)$$

Steady-state ionic balance equations

$$I_{s,Ca}+I_l+I_{cp}+I_{b,Ca}-2I_{NCX} = I_{Ca} = 0, \quad (35)$$

$$I_{s,K}+I_{dr}+I_{ir}+I_{bk}+I_{b,K}-2I_{NaK} = I_K = 0, \quad (36)$$

$$I_{s,Na}+I_{b,Na}+3I_{NCX}+3I_{NaK} = I_{Na} = 0. \quad (37)$$

The work benefited greatly from discussions with Dr. George Christ of WFU and Dr. G. V. Ramanan at AU-KBC.

This work was supported by the Wellcome International Senior Research Fellowship grant No. 070069.

REFERENCES

1. Johnson, P. C. 1986. Autoregulation of blood flow. *Circ. Res.* 59: 483–495.
2. Segal, S. S. 1994. Cell-to-cell communication coordinates blood flow control. *Hypertension.* 23:1113–1120.
3. Schubert, R., and M. J. Mulvany. 1999. The myogenic response: established facts and attractive hypotheses. *Clin. Sci.* (*Lond.*). 96: 313–326.
4. Folkow, B. 1962. Transmural pressure and vascular tone—some aspects of an old controversy. *Arch. Int. Pharmacodyn. Ther.* 139: 455–469.
5. Faraci, F. M., G. L. Baumbach, and D. D. Heistad. 1989. Myogenic mechanisms in the cerebral circulation. *J. Hypertens. Suppl.* 7:S61–S64.
6. Muller, J. M., M. J. Davis, and W. M. Chilian. 1996. Integrated regulation of pressure and flow in the coronary microcirculation. *Cardiovasc. Res.* 32:668–678.
7. Knot, H. J., N. B. Standen, and M. T. Nelson. 1998. Ryanodine receptors regulate arterial diameter and wall [Ca^{2+}] in cerebral arteries of rat via Ca^{2+}-dependent K^+ channels. *J. Physiol.* 508:211–221.
8. Bayliss, W. M. 1902. On the local reactions of the arterial wall to changes of internal pressure. *J. Physiol.* 28:220–231.
9. Harder, D. R. 1984. Pressure-dependent membrane depolarization in cat middle cerebral artery. *Circ. Res.* 55:197–202.
10. Knot, H. J., and M. T. Nelson. 1998. Regulation of arterial diameter and wall [Ca^{2+}] in cerebral arteries of rat by membrane potential and intravascular pressure. *J. Physiol.* 508:199–209.
11. Welsh, D. G., A. D. Morielli, M. T. Nelson, and J. E. Brayden. 2002. Transient receptor potential channels regulate myogenic tone of resistance arteries. *Circ. Res.* 90:248–250.
12. Hill, M. A., H. Zou, J. Simon, S. J. Potocnik, G. A. Meininger, and M. J. Davis. 2001. Arteriolar smooth muscle mechanotransduction: Ca^{2+} signaling pathways underlying myogenic reactivity. *J. Appl. Physiol.* 91: 973–983.

13. Borgstrom, P., and P. O. Grande. 1979. Myogenic microvascular responses to change of transmural pressure. A mathematical approach. *Acta Physiol. Scand.* 106:411–423.

14. Borgstrom, P., P. O. Grande, and S. Mellander. 1982. A mathematical description of the myogenic response in the microcirculation. *Acta Physiol. Scand.* 116:363–376.

15. Hai, C. M., and R. A. Murphy. 1988. Cross-bridge phosphorylation and regulation of latch state in smooth muscle. *Am. J. Physiol.* 254: C99–C106.

16. Lee, S., and G. W. Schmid-Schonbein. 1996. Biomechanical model for the myogenic response in the microcirculation: Part I. Formulation and initial testing. *J. Biomech. Eng.* 118:145–151.

17. Parthimos, D., D. H. Edwards, and T. M. Griffith. 1999. Minimal model of arterial chaos generated by coupled intracellular and membrane Ca^{2+} oscillators. *Am. J. Physiol.* 277:1119–1144.

18. Yang, J., J. W. Clark, Jr., R. M. Bryan, and C. Robertson. 2003. The myogenic response in isolated rat cerebrovascular arteries: smooth muscle cell model. *Med. Eng. Phys.* 25:691–709.

19. Yang, J., J. W. Clark, Jr., R. M. Bryan, and C. Robertson. 2003. The myogenic response in isolated rat cerebrovascular arteries: vessel model. *Med. Eng. Phys.* 25:711–717.

20. Hill, M. A., H. Zou, M. J. Davis, S. J. Potocnik, and S. Price. 2000. Transient increases in diameter and $[Ca^{2+}]_i$ are not obligatory for myogenic constriction Am. *J. Physiol.* 278:345–352.

21. Nelson, M. T., H. Cheng, M. Rubart, L. F. Santana, A. D. Bonev, H. J. Knot, and W. J. Lederer. 1995. Relaxation of arterial smooth muscle by calcium sparks. *Science.* 270:633–637.

22. ZhuGe, R., K. E. Fogarty, R. A. Tuft, and J. V. Walsh, Jr. 2002. Spontaneous transient outward currents arise from microdomains where BK channels are exposed to a mean Ca^{2+} concentration on the order of 10 μM during a Ca^{2+} spark. *J. Gen. Physiol.* 120:15–28.

23. Jaggar, J. 2001. Intravascular pressure regulates local and global Ca^{2+} signaling in cerebral artery smooth muscle cells. *Am. J. Physiol.* 281: 439–448.

24. Rubart, M., J. B. Patlak, and M. T. Nelson. 1996. Ca^{2+} currents in cerebral artery smooth muscle cells of rat at physiological Ca^{2+} concentrations. *J. Gen. Physiol.* 107:459–472.

25. Schuhmann, K., C. Romanin, W. Baumgartner, and K. Groschner. 1997. Intracellular Ca^{2+} inhibits smooth muscle L-type Ca^{2+} channels by activation of protein phosphatase type 2B and by direct Interaction with the channel. *J. Gen. Physiol.* 110:503–513.

26. Luo, C. H., and Y. Rudy. 1994. A dynamic model of the cardiac ventricular action potential. I. Simulations of ionic currents and concentration changes. *Circ. Res.* 74:1071–1096.

27. Luo, C. H., and Y. Rudy. 1994. A dynamic model of the cardiac ventricular action potential. II. Afterdepolarizations, triggered activity, and potentiation. *Circ. Res.* 74:1097–1113.

28. Kirber, M. T., J. V. Walsh, Jr., and J. J. Singer. 1988. Stretch-activated ion channels in smooth muscle: a mechanism for the initiation of stretch-induced contraction. *Pflugers Arch.* 412:339–345.

29. Earley, S., B. J. Waldron, and J. E. Brayden. 2004. Critical role for transient receptor potential channel TRPM4 in myogenic constriction of cerebral arteries. *Circ. Res.* 95:922–929.

30. Wu, X., and M. J. Davis. 2001. Characterization of stretch-activated cation current in coronary smooth muscle cells. *Am. J. Physiol.* 280: 1751–1761.

31. Davis, M. J., J. A. Donovitz, and J. D. Hood. 1992. Stretch-activated single-channel and whole cell currents in vascular smooth muscle cells. *Am. J. Physiol.* 262:1083–1088.

32. Eggermont, J. A., M. Vrolix, L. Raeymaekers, F. Wuytack, and R. Casteels. 1988. Ca^{2+}-transport ATPases of vascular smooth muscle. *Circ. Res.* 62:266–278.

33. O'Donnell, M. E., and N. E. Owen. 1994. Regulation of ion pumps and carriers in vascular smooth muscle. *Physiol. Rev.* 74:683–721.

34. Caride, A. J., A. R. Penheiter, A. G. Filoteo, Z. Bajzer, A. Enyedi, and J. T. Penniston. 2001. The plasma membrane calcium pump displays memory of past calcium spikes. *J. Biol. Chem.* 276:39797–39804.

35. Fayazi, A. H., S. A. Lapidot, B. K. Huang, R. W. Tucker, and R. D. Phair. 1996. Resolution of the basal plasma membrane calcium flux in vascular smooth muscle cells. *Am. J. Physiol.* 270:H1972–H1978.

36. Karaki, H., H. Ozaki, M. Hori, M. Mitsui-Saito, K. Amano, K. Harada, S. Miyamoto, H. Nakazawa, K. Won, and K. Sato. 1997. Calcium movements, distribution, and functions in smooth muscle. *Pharmacol. Rev.* 49:157–230.

37. Blaustein, M. P., and W. J. Lederer. 1999. Sodium/calcium exchange: its physiological implications. *Physiol. Rev.* 79:763–854.

38. Varghese, A., and G. R. Sell. 1997. A conservation principle and its effect on the formulation of Na-Ca exchanger current in cardiac cells. *J. Theor. Biol.* 189:33–40.

39. Faber, G. M., and Y. Rudy. 2000. Action potential and contractility changes in $[Na^+]_i$ overloaded cardiac myocytes: a simulation study. *Biophys. J.* 78:2392–2404.

40. Fontana, G., R. S. Rogowski, and M. P. Blaustein. 1995. Kinetic properties of the sodium-calcium exchanger in rat brain synaptosomes. *J. Physiol.* 485:349–364.

41. Kamishima, T., and G. McCarron. 1998. Ca^{2+} removal mechanisms in rat cerebral resistance size arteries. *Biophys. J.* 75:1767–1773.

42. Nelson, M. T., and J. M. Quayle. 1995. Physiological roles and properties of potassium channels in arterial smooth muscle. *Am. J. Physiol.* 268:799–822.

43. Volk, K. A., J. J. Matsuda, and E. F. Shibata. 1991. A voltage-dependent potassium current in rabbit coronary artery smooth muscle cells. *J. Physiol.* 439:751–768.

44. Quayle, J. M., C. Dart, and N. B. Standen. 1996. The properties and distribution of inward rectifier potassium currents in pig coronary arterial smooth muscle. *J. Physiol.* 494:715–726.

45. Wang, Y., and D. A. Mathers. 1993. Ca^{2+}-dependent K^+ channels of high conductance in smooth muscle cells isolated from rat cerebral arteries. *J. Physiol.* 462:529–545.

46. Perez, G. J., A. D. Bonev, and M. T. Nelson. 2001. Micromolar Ca^{2+} from sparks activates Ca^{2+}-sensitive K^+ channels in rat cerebral artery smooth muscle. *Am. J. Physiol.* 281:1769–1775.

47. Nakamura, Y., Y. Ohya, I. Abe, and M. Fujishima. 1999. Sodium-potassium pump current in smooth muscle cells from mesenteric resistance arteries of the Guinea-pig. *J. Physiol.* 519:203–212.

48. VanBavel, E., and M. J. Mulvany. 1994. Role of wall tension in the vasoconstrictor response of cannulated rat mesenteric small arteries. *J. Physiol.* 477:103–115.

49. Ingber, D. E. 2006. Cellular mechanotransduction: putting all the pieces together again. *FASEB J.* 20:811–827.

50. Rizzoni, D., E. Porteri, A. Piccoli, M. Castellano, G. Bettoni, M. L. Muiesan, G. Pasini, V. Guelfi, M. J. Mulvany, and E. A. Rosei. 1998. Effects of Losartan and Enalapril on small artery structure in hypertensive rats. *Hypertension.* 32:305–310.

51. Mulvany, M. J., C. Aalkjaer, and T. T. Petersen. 1984. Intracellular sodium, membrane potential, and contractility of rat mesenteric small arteries. *Circ. Res.* 54:740–749.

52. Lamont, C., T. V. Burdyga, and S. Wray. 1998. Intercellular Na^+ measurements in smooth muscle using SBFI—changes in $[Na^+]$, Ca^{2+} and force in normal and Na^+-loaded ureter. *Pflugers Arch.* 435: 523–527.

53. Ye, M., G. Flores, and D. Batlle. 1996. Angiotensin II and Angiotensin-(1–7) effects on free cytosolic sodium, intracellular pH, and the Na^+-H^+ antiporter in vascular smooth muscle. *Hypertension.* 27:72–78.

54. Chilton, L., and R. Loutzenhiser. 2001. Functional evidence for an inward rectifier potassium current in rat renal afferent arterioles. *Circ. Res.* 88:152–158.

55. Wu, C., and C. H. Fry. 2001. Na^+/Ca^{2+} exchange and its role in intracellular Ca^{2+} regulation in Guinea-pig detrusor smooth muscle. *Am. J. Physiol.* 280:1090–1096.

56. Jiang, Z., J. Si, M. R. Lasarev, and A. L. Nuttall. 2001. Two resting potential levels regulated by the inward-rectifier potassium channel in the Guinea-pig spiral modiolar artery. *J. Physiol.* 537:829–842.

57. Osol, G., J. F. Brekke, K. McElroy-Yaggy, and N. I. Gokina. 2002. Myogenic tone, reactivity, and forced dilatation: a three-phase model of in vitro arterial myogenic behavior. *Am. J. Physiol.* 283:2260–2267.

58. McCarron, J. G., and W. Halpern. 1990. Potassium dilates rat cerebral arteries by two independent mechanisms. *J. Physiol.* 430:389–398.

59. Knot, H. J., and M. T. Nelson. 1995. Regulation of membrane potential and diameter by voltage-dependent K^+ channels in rabbit myogenic cerebral arteries. *Am. J. Physiol.* 269:348–355.

60. Gadsby, D., and M. Nakao. 1989. Steady-state current-voltage relationship of the Na/K pump in Guinea-pig ventricular myocytes. *J. Gen. Physiol.* 94:511–537.

61. Batlle, D. C., M. Godinich, M. LaPointe, E. Munoz, F. Carone, and N. Mehring. 1991. Extracellular Na^+ dependency of free cytosolic Ca^{2+} in aortic vascular smooth muscle cells. *Am. J. Physiol.* 261:C845–C856.

62. Nelson, M. T., M. A. Conway, H. J. Knot, and J. E. Brayden. 1997. Chloride channel blockers inhibit myogenic tone in rat cerebral arteries. *J. Physiol.* 502:259–264.

63. Raina, H., S. Potocnik, N. Kotecha, and M. A. Hill. 2004. Na^+/Ca^{2+} (NCX) exchange in myogenically active arterioles. *In* Proceedings of the 8th International Symposium on Resistance Arteries. D. Henrion, editor. Karger, Basel, Switzerland.

64. Watanabe, J., S. Horiguchi, M. Keitoku, A. Karibe, M. Takeuchi, S. Suzuki, S. Satoh, and K. Shirato. 1996. The role of extracellular cations in the development of myogenic contraction in isolated rat small arteries. *Jpn. Circ. J.* 60:239–246.

65. Carl, A., H. K. Lee, and K. M. Sanders. 1996. Regulation of ion channels in smooth muscles by calcium. *Am. J. Physiol.* 271:9–34.

66. Jackson, W. F. 2000. Ion channels and vascular tone. *Hypertension.* 35:173–178.

67. Kleppisch, T., and M. T. Nelson. 1995. Adenosine activates ATP-sensitive potassium channels in arterial myocytes via A2 receptors and cAMP-dependent protein kinase. *Proc. Natl. Acad. Sci. USA.* 92: 12441–12445.